Magnetotransport in overdoped $La_{2-x}Sr_xCuO_4$: Effect of anisotropic scattering

Rui-Ying Mao,[1] Da Wang,[1,2,*] and Qiang-Hua Wang[1,2,†]

[1]*National Laboratory of Solid State Microstructures & School of Physics, Nanjing University, Nanjing 210093, China*

[2]*Collaborative Innovation Center of Advanced Microstructures, Nanjing University, Nanjing 210093, China*

(Received 22 July 2022; revised 28 September 2022; accepted 30 November 2022; published 8 December 2022)

We revisit the Hall effect and magnetoresistivity by incorporating the anisotropic scattering caused by apical oxygen vacancies in overdoped La-based cuprates. The theoretical calculations within the Fermi liquid picture agree well with a handful of anomalous magnetotransport data, better than the results using an isotropic scattering rate alone. In particular, we obtain the upturn of Hall coefficient R_H with decreasing temperature T, the initial drop of R_H in magnetic field B in all overdoped regimes, the linear resistivity ρ versus B near the van Hove doping level, the temperature dependence of the magnetoresistivity ratio, and the violation of Kohler's law. These results suggest that many of the anomalous transport behaviors in overdoped $La_{2-x}Sr_xCuO_4$ could actually be understood within the Fermi liquid picture.

DOI: 10.1103/PhysRevB.106.235111

I. INTRODUCTION

As the first family of high temperature superconductors discovered so far, cuprates continue to challenge our understanding of many body physics, in particular the properties of a doped Mott insulator [1]. However, it is hoped that at least in the overdoped regime, the correlation effect might be weakened relatively, such that a Fermi liquid picture could be applied. On this basis, the superconducting state could also be described properly by the Bardeen-Cooper-Schrieffer (BCS) theory. If this were the case, we would have a good starting point to descriminate what falls within/beyond the Fermi liquid theory at lower doping levels [2]. The crossover doping level above which the Fermi liquid picture applies is not yet clear, and in fact, many anomalous phenomena reported in recent expeiments seem to push the "boundary" of the Fermi liquid phase to very high doping levels, even beyond the superconducting domes [3]. To gain further insights, it is important to investigate the anomalies more closely to see whether and how they could actually be described within the Fermi liquid picture.

The upturn of the Hall coefficient R_H with decreasing temperature T in overdoped $La_{2-x}Sr_xCuO_4$ (LSCO) [4] is an early signature of the breakdown of the Fermi liquid theory, since within the latter picture R_H should be T independent unless the system has both electronlike and holelike Fermi pockets. The upturn of R_H was later confirmed to persist for all doping levels up to $x = 0.36$ [5]. In particular, at $x = 0.32$, R_H grows continuously from negative to positive values with decreasing temperature. Another signature of the Fermi liquid breakdown comes from the linear resistivity under strong magnetic fields that recovers the normal states from the superconducting state. The T-linear resistivity at low temperatures persists up to $x \approx 0.3$ in LSCO [6], which is surprising since the doping level is readily far from the hypothetic quantum critical point at $x_c \approx 0.2$. Subsequent careful analysis of the magnetoresistivity data at $x = 0.23$ reveals a special quadratic scaling [7] consistent with the phenomenological "quadrature Planckian" dissipation $\tau^{-1} = \sqrt{T^2 + \gamma^2 B^2}$ [8]. This includes an unusual resistivity linear in B at low temperatures [9]. In LSCO, the Fermi surface changes from being holelike to electron-like as the doping level increases through the van Hove singularity (VHS) at $x_{\rm vhs} = 0.2$. One expects a corresponding change in the Hall coefficient. Indeed, in the strong field limit, $R_H = 1/(1+x)e$ for $x < x_{\rm vhs}$, and $-1/(1-x)e$ for $x > x_{\rm vhs}$, respectively [10]. However, in the weak field limit, R_H is found to smoothly decrease with doping, from positive to negative values, and changes sign at $x_0 \approx 0.3$ [5]. Recently, these behaviors are qualitatively reproduced within the Fermi liquid picture under an isotropic scattering rate [11].

On the other hand, in the superconducting state of overdoped LSCO films, the low temperature superfluid density ρ_s is found to decrease linearly with T [12], which is the expected behavior of a clean d-wave superconductor [13]. However, the zero temperature superfluid density $\rho_s(0)$ is found to scale linearly with the transition temperature T_c, which is instead a typical behavior of a dirty BCS superconductor [14]. This dilemma is reconciled only recently by the recognition of the unique property of apical oxygen vacancies [15]. Such impurities are known to be more populated with overdoping [16]. In the Born limit, they cause an anisotropic scattering rate $\Gamma_d \cos^2(2\theta)$ (with θ the azimuthal angle relative to the anti-nodal direction) through second-order hopping processes connecting the nearest neighboring sites [15]. The global scale of the scattering rate affects the transition temperature, hence can produce the behavior $\rho_s(0) \propto T_c$ in the dirty limit. The depletion of the superfluid density at low temperatures are contributed by nodal quasiparticle excitations, but since the above form of scattering rate vanishes in the nodal direction, the behavior is similar to what would be found in the clean limit, even if the global scale sets the system in the dirty limit. This solves the puzzle regarding

*dawang@nju.edu.cn
†qhwang@nju.edu.cn

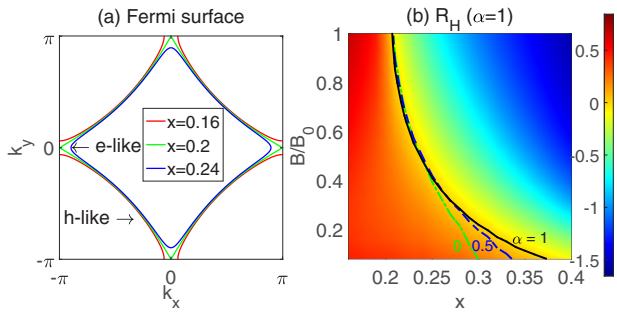

FIG. 1. (a) Fermi surface for three doping levels near the VHS doping $x_{\rm vhs}$. (b) R_H as a function of x and B. The color encodes the value of R_H for $\alpha = 1$, and the black curve is the contour across which R_H changes sign. The same contour for $\alpha = 0.5$ (dashed blue line) and 0 (dashed-dotted green line) are also shown for comparison.

the two linear scaling behaviors of the superfluid density [15]. Furthermore, such an anisotropic scattering suggests that the optical conductivity (versus the frequency) is an integration of Lorentzians over a distribution of scattering rates, hence becomes increasingly sharp as the frequency approaches zero. Therefore a single-mode Lorentzian fit of the optical conductivity data at finite frequency would underestimate the Drude weight [15]. This resolves the so-called "missing" of Drude weight upon overdoping [17].

In view of the important effect of the anisotropic scattering rate, we are motivated to reexamine the magnetotransport in overdoped LSCO, so far only considered theoretically in the isotropic scattering limit [11]. We find that incorporating the anisotropic scattering rate further provides better agreement with a handful of experiments, such as the the upturn of R_H with decreasing T [4,5], the initial drop of R_H in B for all overdopings [18,19], the linear resistivity ρ versus B [6,9], the temperature dependence of the magnetoresistivity ratio $[\rho(B) - \rho(0)]/\rho(0)$ [6,9,20,21], and the violation of Kohler's law [20,21]. These results suggest that many of the anomalous transport behaviors in overdoped LSCO could actually be understood within the Fermi liquid picture.

II. MODEL AND METHODS

The band structure of overdoped LSCO as obtained from angle-resolved photoemission spectroscopy (ARPES) can be described quite well by a one-band tight-binding model defined on the square lattice with hoppings t, $t' = -0.12t$ and $t'' = 0.06t$ between the first, second, and third nearest neighboring sites [22,23]. For simplicity, we assume a purely two-dimensional rigid band structure, i.e., only the chemical potential μ is to be tuned to match the doping level. In this model, there is a VHS at $x_{\rm vhs} \approx 0.197$, across which the Fermi surface (FS) topology changes from hole to electronlike, as shown in Fig. 1(a).

Throughout this work, the magnetic field $\mathbf{B}$ is assumed to be perpendicular to the basal plane, which is the same as in most experiments. According to the Luttinger theorem [24], the enclosed area of the FS is $(1 + x)S_{\rm BZ}/2$ ($\mathcal{S}_{\rm BZ}$ the Brillouin zone area) for $x < x_{\rm vhs}$ and $(1 - x)S_{\rm BZ}/2$ for $x > x_{\rm vhs}$, which gives rise to the Hall coefficient $R_H = 1/(1 + x)e$ and $-1/(1 - x)e$, respectively, in the strong field limit $B \to \infty$ [10]. However, in the weak field limit, the Hall coefficient loses the above topological meaning (unless in the continuum limit or a band with quadratic dispersion) and instead should be determined by the Fermi surface curvature as clarified geometrically by Ong [25], or equivalently captured by the Kubo formula for the longitudinal conductivity

$$\sigma_{xx} = \frac{2e^2}{N_k} \sum_{\mathbf{k}} \tau(\mathbf{k}) v_x^2(\mathbf{k}) \left(-\frac{\partial f}{\partial \varepsilon_{\mathbf{k}}} \right), \tag{1}$$

where 2 comes from spin, and the Hall conductivity

$$\sigma_{xy} = -\frac{2e^3 B}{N_k} \sum_{\mathbf{k}} \tau^2(\mathbf{k}) v_x \left(v_x \frac{\partial v_y}{\partial k_y} - v_y \frac{\partial v_y}{\partial k_x} \right) \left(-\frac{\partial f}{\partial \varepsilon_{\mathbf{k}}} \right), \tag{2}$$

where $v_{x,y} = \partial \varepsilon_{\mathbf{k}} / \partial k_{x,y}$ and f is the Fermi distribution function. The collision time $\tau(\mathbf{k})$ is the inverse of the total scattering rate given by

$$\tau^{-1}(\mathbf{k}) = \Gamma_s + \tfrac{1}{4}\Gamma_d (\cos k_x - \cos k_y)^2, \tag{3}$$

where Γ_s and Γ_d are isotropic and anisotropic scattering amplitudes. We assume the Γ_d-term arises from the apical oxygen vacancies in overdoped LSCO [15]. (Below the optimal doping level, the anisotropic scattering is also proposed in the phenomenological "cold spot" model [26]. But here we will limit ourselves to over doping only, as it might be hopeless to apply the Fermi liquid theory below optimal doping, where the strong correlation effects beyond the Fermi liquid picture are known to be essential.) In the following, we introduce a dimensionless parameter α to quantify the anisotropy fraction such that $\Gamma_d = \alpha\Gamma_0$ and $\Gamma_s = (1 - \alpha)\Gamma_0$, with $\Gamma_0 = \Gamma_s + \Gamma_d$. We note that in Eq. (2) the Hall conductivity σ_{xy} is proportional to $e^3 B$. This should be compared to the quantized Hall conductivity in unit of e^2/h in two-dimensional quantum Hall systems or Chen insulators.

The Kubo formula is applicable in the limit of $B \to 0$. In order to go beyond the B-linear Hall conductivity, we adopt the Chambers' formula [27]

$$\sigma_{\alpha\beta} = \frac{2e^3 B}{(2\pi)^2} \int \mathrm{d}\varepsilon \left(-\frac{\partial f}{\partial \varepsilon} \right) \int_0^{\mathcal{T}} \mathrm{d}t\, v_\alpha[\mathbf{k}(t)] \times \int_{-\infty}^{t} \mathrm{d}t'\, v_\beta[\mathbf{k}(t')] \exp\left\{ -\int_{t'}^{t} \frac{\mathrm{d}s}{\tau[\mathbf{k}(s)]} \right\}, \tag{4}$$

which can be derived from the Boltzmann transport equation [28,29]. Within the semiclassical picture, the electrons are driven by the Lorentz force $\dot{\mathbf{k}} = -e\mathbf{v}_{\mathbf{k}} \times \mathbf{B}$ and move on cyclotron orbits in the momentum space. This semiclassical picture can be justified by the observation of cyclotron resonance in LSCO [30]. At low temperatures, the cyclotron orbit is limited on the Fermi surface (because of the derivative of the Fermi function in the above formula). We obtain the time-dependent momentum $\mathbf{k}(t)$, velocity $\mathbf{v}(t)$, and lifetime $\tau(t)$. Since both $\mathbf{v}(t)$ and $\tau(t)$ are periodic functions with the cyclotron period $\mathcal{T}$, the integral over t' can be performed

within each period, yielding

$$\sigma_{\alpha\beta} = \frac{2e^3 B}{(2\pi)^2}\left[1 - \exp\left(-\int_0^{\mathcal{T}} \frac{ds}{\tau(s)}\right)\right]^{-1} \times \int_0^{\mathcal{T}} dt\, v_\alpha(t) \int_{t-\mathcal{T}}^{t} dt'\, v_\beta(t') \exp\left[-\int_{t'}^{t} \frac{ds}{\tau(s)}\right], \quad (5)$$

which is convenient for numerical calculations [31]. Using Eq. (5) we calculate both σ_{xx} and σ_{xy}. The conductivity tensor is then reversed to obtain the longitudinal resistivity ρ_{xx} (denoted by ρ for simplicity) and Hall coefficient R_H,

$$\begin{bmatrix} \rho & -R_H B \\ R_H B & \rho \end{bmatrix} = \begin{bmatrix} \sigma_{xx} & \sigma_{xy} \\ -\sigma_{xy} & \sigma_{xx} \end{bmatrix}^{-1}. \quad (6)$$

To quantify the magnetic field, we define a characteristic magnetic field $B_0 = m_c^*/e\tau$ with $\tau = 1/\Gamma_0$ a time scale and $m_c^* = 1/ta^2$ a mass scale (a is the lattice constant). As a rough estimation, we have $B_0 \sim 100$ T for LSCO [11]. In the following, we use the Kubo formula for $B/B_0 \to 0$, while the results for finite $B/B_0 > 0.002$ are obtained by the Chambers formula. The latter can be applied for any nonzero B, but becomes numerically inefficient in the limit of $B/B_0 \to 0$.

III. RESULTS

A. Hall coefficient

We first consider the doping and magnetic field dependence in R_H (at low temperatures). The numerical result is shown in Fig. 1(b). The color scale shows the value of R_H for a purely anisotropic scattering, $\alpha = 1$. The solid black line highlights where R_H changes sign. In the strong field limit, where $\mathcal{T} \to 0$, R_H changes abruptly from $1/(1+x)$ at $x < x_{\rm vhs}$ to $-1/(1-x)$ at $x > x_{\rm vhs}$. This behavior is independent of the scattering anisotropy, as the system is effectively in the ballistic regime, such that the Hall conductivity is purely determined by the Luttinger volume enclosed by the Fermi surface [10]. As the field decreases, the cyclotron motion becomes slow and sensitive to the local scattering rate. As a result, the conductivity tensor becomes sensitive to the local curvature of the Fermi surface. The full cyclotron motion can be decomposed into segments. Near the nodal point, the quasiparticle moves on a holelike segment in our doping range, while near the antinodal point, the quasiparticle moves on electronlike segment for $x > x_{\rm vhs}$, see Fig. 1(a). The total conductivity tensor is given by a weighted sum of the segments. For the anisotropy fraction $\alpha = 1$, the nodal quasiparticles experience vanishing scattering, hence make leading contribution to the conductivity. This explains why $R_H > 0$ for all x near and above $x_{\rm vhs}$. For even higher doping levels, the electron-like segment increases and eventually R_H becomes negative. This explains the sign change of R_H with increasing doping at low fields. For comparison, we also present the transition lines (where R_H changes sign) for scattering anisotropy $\alpha = 0.5$ (dashed blue line) and 0 (dotted-dashed green line) in Fig. 1(b). We see the transition doping level is higher for larger scattering anisotropy. This is because a larger anisotropy enhances more strongly the relative contribution of the holelike nodal quasiparticles to the conductivity tensor.

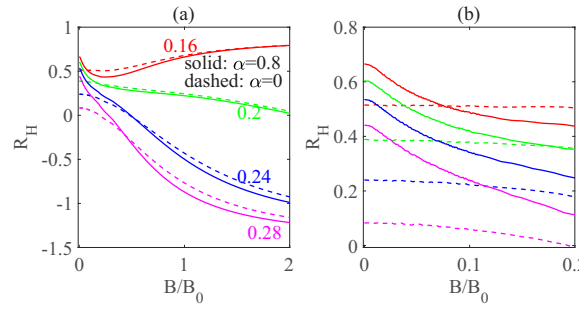

FIG. 2. Magnetic field dependence of R_H in the case of $\alpha = 0.8$ (solid lines) and $\alpha = 0$ (dashed lines) at four different doping levels $x = 0.16, 0.2, 0.24, 0.28$. (b) is a zooming of (a) at low fields.

For moderate fields, R_H should interpolate between the high and weak field limits. This is roughly the case in Fig. 1(b). Interestingly, closer examination of our results reveal an interesting structure in the evolution of R_H: it always drops with B at small fields, and drops more quickly as the scattering anisotropy α increases, see Figs. 2(a) and 2(b). This initial drop of R_H in B happens for all doping levels on the two sides of the VHS, and is consistent with the experiments [18,19] that appeared puzzling beforehand. To gain qualitative insights, we consider an effective "two band" model [32], in which the two bands should be understood as two types of segments near the nodal and antinodal points. In this simplified model, the total Hall coefficient can be calculated up to the B^2 term,

$$R_H = \frac{\rho_1^2 R_2 + \rho_2^2 R_1 + R_1 R_2 (R_1 + R_2) B^2}{(\rho_1 + \rho_2)^2 + (R_1 + R_2)^2 B^2} \approx \frac{\rho_1^2 R_2 + \rho_2 R_1^2}{(\rho_1 + \rho_2)^2} - \frac{(R_1 + R_2)(\rho_1 R_2 + \rho_2 R_1)^2}{(\rho_1 + \rho_2)^4} B^2, \quad (7)$$

where $R_{1,2}$ and $\rho_{1,2}$ are Hall coefficient and resistivity for the two bands, respectively. As long as $R_1 + R_2 > 0$, which is clearly true for $x < x_{\rm vhs}$ since both R_1 and R_2 are positive, R_H drops with B. While for $x > x_{\rm vhs}$, the holelike segment is much larger than electronlike one in our range $x < 0.4$, so we still have $R_1 + R_2 > 0$. This qualitative picture of the initial drop of R_H in B is consistent with our numerical results shown in Fig. 2(a). The quadratic dependence at small B is dictated by time-reversal symmetry, and is also correctly reproduced in Fig. 2(b). Therefore, the initial drop of R_H in B is a universal feature in our doping range ($0.16 < x < 0.4$) on both sides of the VHS. Furthermore, by comparing the results of $\alpha = 0$ and $\alpha = 0.8$, see Fig. 2, the anisotropic scattering is found to make a steeper initial drop (at finite but small B), in better agreement with the experiments [18,19].

We now consider the temperature dependence of R_H. The experimental data of R_H [5] in unit of $a^2 c/e$ are shown as dots in Fig. 3(a), where $a = 3.8$Å and $c = 6.6$Å are lattice constants of LSCO [23] and e is the electron charge. For each temperature and doping, we tune the anisotropy ratio α to fit the experimental data of R_H. The fitted results of α are shown as dots in Fig. 3(b). At high temperature, we cannot fit the experimental data within a reasonable range $\alpha \in [0, 1]$, which are represented by open circles.

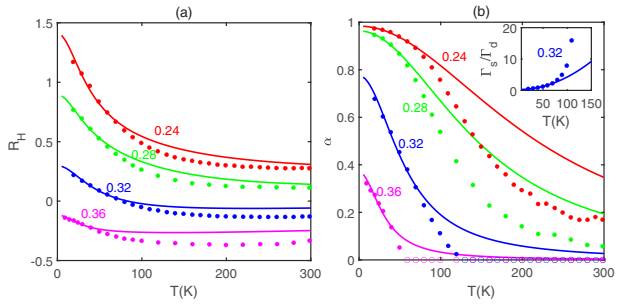

FIG. 3. The experimental data [5] of R_H (in unit of a^2c/e) versus temperature T, shown as dots in (a), are fitted point-by-point to extract the anisotropy ratio α shown in (b). The solid lines in (a) and (b) are fits to the symbols by assuming $\Gamma_s = \Gamma_{s0} + gT^2$. The doping level is indicated on the colored line. The inset in (b) plots Γ_s/Γ_d versus T at $x = 0.32$. The open circles in (b) indicate the temperatures at which the fit to the data (not shown) fails to obtain an $\alpha \in [0, 1]$.

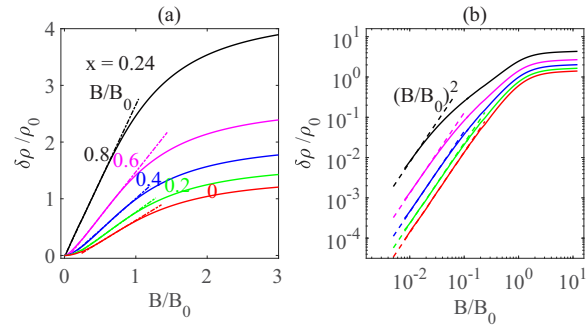

FIG. 4. (a) The magnetoresistivity ratio $\delta\rho/\rho_0$ are plotted versus B at $x = 0.24$ for $\alpha = 0, 0.2, \ldots, 0.8$. The dashed lines show B-linear fits for the intermediate fields. (b) is the same as (a) but presented in log-log scale to reveal the B^2 behavior at low fields (highlighted by dashed lines).

To understand the temperature dependence in R_H as well as in α, we assume the isotropic part, Γ_s, receives Fermi-liquid correction from electron-electron interactions. It therefore decreases as the temperature is lowered. On the other hand, the anisotropic part, Γ_d, is caused by apical oxygen vacancies, hence is independent of the temperature. Therefore, the scattering anisotropy $\alpha = \Gamma_d/(\Gamma_d + \Gamma_s)$ is expected to increase as the temperature is lowered. As a result, the holelike contribution to R_H from nodal quasiparticles becomes larger relatively. This provides a mechanism for the upturn of R_H as the temperature is lowered.

To see how this scenario works, we assume $\Gamma_s = \Gamma_{s0} + gT^2$ and $\Gamma_d = \Gamma_{d0}$, correspondingly $\alpha^{-1} = 1 + \Gamma_s/\Gamma_d$, to fit the symbols in both panels of Fig. 3. Note that the total scattering rate $\Gamma_s + \Gamma_d$ has no effect on R_H, but only their ratio $\Gamma_s\Gamma_d$ determines R_H at each doping. The fitted results of R_H are presented as solid lines. We observe fair agreement between the dots and the solid lines at low temperatures. In particular, the inset of Fig. 3(b) plots Γ_s/Γ_d versus T in the case of $x = 0.32$. The T^2 dependence at low temperatures is obvious. We notice that the T dependence of α has been pointed out in Refs. [33,34]. On the other hand, the upturn of R_H becomes even more significant upon underdoping [4,5], where the mechanism should go beyond the Fermi-liquid picture because of the emergence of the pseudogap.

B. Magnetoresistivity

We now discuss the field dependence of the resistivity, or magnetoresistivity. Previously, we found that the proximity to the VHS can lead to quasilinear dependence of the resistivity ρ in a sizable window of intermediate magnetic field B [11], in qualitative agreement with the experiment [9]. At that stage the simplest isotropic scattering was assumed. Here we examine further the effect of the anisotropic scattering Γ_d. In Fig. 4(a), the dimensionless magnetoresistivity ratio $\delta\rho/\rho_0 = [\rho(B) - \rho(0)]/\rho(0)$ is plotted versus the field for several values of α. Fig. 4(b) is a replot of Fig. 4(a) in the log-log scale. These results show that the magnetoresistivity is quadratic in B at small fields, quasi-linear in intermediate fields, and saturates at high fields. In comparison to the case of $\alpha = 0$ (isotropic scattering), we see that a larger anisotropy reduces the B^2 regime on one hand, and enhances the saturation value in the large field limit on the other hand. Therefore, the intermediate crossover (quasi B-linear) regime is enlarged by a larger α. If we assume that α becomes effectively larger as the temperature is lowered, as we discussed in the previous subsection, the above result implies the B-linear regime extends as the temperature is lowered, consistent with the experimental results [6,9]. This adds salt to the conventional mechanism based on the cyclotron motion [11,34,35], which should be compared to the more exotic picture of "quadrature Planckian dissipation" [7,8,36].

The above result can also be related to the so-called Kohler's law, which says that the magnetoresistivity ratio $\delta\rho/\rho_0$ is a universal function of B/ρ_0. This is true only if α does not change with temperature such that the data at different temperatures fall on the same line. But in LSCO, since α grows as the temperature is lowered (see the previous subsection), the Kohler's law is expected to be violated more quickly at lower temperatures. On the other hand, a larger value of α also leads to a larger slope in $\delta\rho/\rho_0$ as a function of B in the intermediate linear regime (which actually extends to very small fields), see Fig. 4(a). These features are consistent with the experiments [20,21]. Therefore, variation of the scattering anisotropy in temperature provides a plausible explanation of the violation of Kohler's law.

Finally, we examine the doping dependence of the magnetoresistivity. In Fig. 5, we plot the saturated magnetoresistivity ratio $\delta\rho_\infty/\rho_0$ versus x for some specific values of α. We see that it increases as the VHS doping is approached. This behavior is caused by the doping dependence of the cyclotron mass, which diverges at the VHS, as shown in our previous work [11]. Here, we see that the magnetoresistivity ratio is further enhanced by the scattering anisotropy. The magnetoresistivity ratio peaks at the VHS, and the global scale clearly grows for larger α (at lower temperature in our picture). These predictions are to be checked in experiments. Our results may also shed light on the experiments [6,9,20,21], where the magnetoresistivity ratio was found to increase at lower temperatures, although the peak at the VHS has not been observed (possibly because the VHS is smeared by the dispersion in k_z, or because the magnetic field is not strong enough).

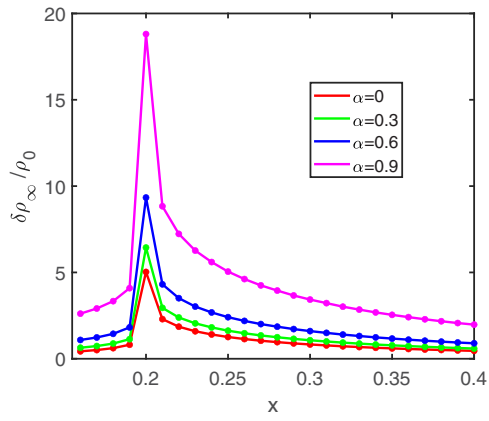

FIG. 5. Doping dependence of the saturated magnetoresistivity ratio $\delta\rho_\infty/\rho_0$ by fixing $\alpha = 0$, 0.3, 0.6, and 0.9, respectively.

IV. SUMMARY

In this work, we studied the effect of the anisotropic scattering Γ_d on the Hall coefficient and magnetoresistivity in overdoped LSCO. Our study is based on well-defined quasiparticles in cyclotron motions under the magnetic field. We find that combining the anisotropic scattering, this picture can explain a handful of experimental observations simultaneously: the upturn of R_H at low temperatures [4,5], initial drop of R_H in magnetic field [18,19], linear magnetoresistivity in a window of intermediate field [9], violation of Kohler's law [20,21], and the temperature (and doping) dependence of the magnetoresistivity ratio [6,9,20,21]. These consistencies indicate the Fermi liquid picture is applicable in a substantial range of overdoped LSCO.

A key ingredient in our discussion is the anisotropic scattering, which we assume to follow from apical oxygen vacancies in overdoped LSCO [16] and more details can be found in Ref. [15]. We should also point out that the functional form of the anisotropic scattering has been invoked in earlier literatures, but the origin is quite different. Ioffe and Millis suggested the so-called "cold spot" model with the scattering rate $\sim\cos^2(2\theta)$ caused by dynamic pair fluctuations to explain the optical conductivity in optimally and underdoped regions [26]. Abrahams and Varma also proposed a scattering rate $\sim v_F^{-1}(\theta)$ [37] from the forward scattering caused by interlayer impurities. Signature of anisotropic scattering appears in ARPES [38–43] and magnetotransport [34,35,44] for both overdoped and underdoped samples. Recently, different out-of-plane dopant impurities, such as Sr atoms or farther O vacancies, are also proposed to support anisotropic scatterings via *ab initio* calculations [45]. Our results call for careful analysis of the effect of different anisotropic scatterings not yet covered in this work.

ACKNOWLEDGMENT

D. W. thanks C. Wu for early collaborations on this topic and J. Wu for helpful discussions about experimental details. This work is supported by the National Natural Science Foundation of China (under Grants No. 11874205, No. 12274205, and No. 11574134).

[1] P. A. Lee, N. Nagaosa, and X.-G. Wen, Doping a Mott insulator: Physics of high-temperature superconductivity, Rev. Mod. Phys. **78**, 17 (2006).
[2] B. Keimer, S. A. Kivelson, M. R. Norman, S. Uchida, and J. Zaanen, From quantum matter to high-temperature superconductivity in copper oxides, Nature (London) **518**, 179 (2015).
[3] I. Božović, J. Wu, X. He, and A. Bollinger, What is really extraordinary in cuprate superconductors? Physica C **558**, 30 (2019).
[4] H. Y. Hwang, B. Batlogg, H. Takagi, H. L. Kao, J. Kwo, R. J. Cava, J. J. Krajewski, and W. F. Peck, Scaling of the Temperature Dependent Hall Effect in La2-xSrxCuO4, Phys. Rev. Lett. **72**, 2636 (1994).
[5] I. Tsukada and S. Ono, Negative Hall coefficients of heavily overdoped La2-xSrxCuO4, Phys. Rev. B **74**, 134508 (2006).
[6] R. A. Cooper, Y. Wang, B. Vignolle, O. J. Lipscombe, S. M. Hayden, Y. Tanabe, T. Adachi, Y. Koike, M. Nohara, H. Takagi, C. Proust, and N. E. Hussey, Anomalous Criticality in the Electrical Resistivity of La2-xSrxCuO4, Science **323**, 603 (2009).
[7] M. Berben, J. Ayres, C. Duffy, R. D. H. Hinlopen, Y.-T. Hsu, M. Leroux, I. Gilmutdinov, M. Massoudzadegan, D. Vignolles, Y. Huang, T. Kondo, T. Takeuchi, J. R. Cooper, S. Friedemann, A. Carrington, C. Proust, and N. E. Hussey, Compartmentalizing the cuprate strange metal, arXiv:2203.04867.
[8] J. Ayres, M. Berben, M. Culo, Y.-T. Hsu, E. van Heumen, Y. Huang, J. Zaanen, T. Kondo, T. Takeuchi, J. R. Cooper, C. Putzke, S. Friedemann, A. Carrington, and N. E. Hussey, Incoherent transport across the strange metal regime of overdoped cuprates, Nature (London) **595**, 661 (2021).
[9] P. Giraldo-Gallo, J. A. Galvis, Z. Stegen, K. A. Modic, F. F. Balakirev, J. B. Betts, X. Lian, C. Moir, S. C. Riggs, J. Wu, A. T. Bollinger, X. He, I. Božović, B. J. Ramshaw, R. D. McDonald, G. S. Boebinger, and A. Shekhter, Scale-invariant magnetoresistance in a cuprate superconductor, Science **361**, 479 (2018).
[10] I. M. Lifshitz, M. I. Azbel, and M. I. Kaganov, The theory of galvanomagnetic effects in metals, Sov. Phys. JETP **4**, 41 (1957).
[11] R.-Y. Mao, D. Wang, C. Wu, and Q.-H. Wang, Magnetotransport in overdoped La2-xSrxCuO4: Fermi liquid approach, Phys. Rev. B **104**, 024501 (2021).
[12] I. Božović, X. He, J. Wu, and A. T. Bollinger, Dependence of the critical temperature in overdoped copper oxides on superfluid density, Nature (London) **536**, 309 (2016).
[13] P. J. Hirschfeld and N. Goldenfeld, Effect of strong scattering on the low-temperature penetration depth of a d-wave superconductor, Phys. Rev. B **48**, 4219 (1993).
[14] A. A. Abrikosov and L. P. Gor'kov, Contribution to the theory of superconducting alloys with paramagnetic impurities, Sov. Phys. JETP **12**, 1243 (1961).
[15] D. Wang, J.-Q. Xu, H.-J. Zhang, and Q.-H. Wang, Anisotropic Scattering Caused by Apical Oxygen Vacancies in Thin Films

of Overdoped High-Temperature Cuprate Superconductors, Phys. Rev. Lett. **128**, 137001 (2022).

[16] G. Kim, G. Christiani, G. Logvenov, S. Choi, H.-H. Kim, M. Minola, and B. Keimer, Selective formation of apical oxygen vacancies in La2-xSrxCuO4, Phys. Rev. Mater. **1**, 054801 (2017).

[17] F. Mahmood, X. He, I. Božović, and N. P. Armitage, Locating the Missing Superconducting Electrons in the Overdoped Cuprates La2-xSrxCuO4, Phys. Rev. Lett. **122**, 027003 (2019).

[18] F. F. Balakirev, J. B. Betts, A. Migliori, I. Tsukada, Y. Ando, and G. S. Boebinger, Quantum Phase Transition in the Magnetic-Field-Induced Normal State of Optimum-Doped High-Tc Cuprate Superconductors at Low Temperatures, Phys. Rev. Lett. **102**, 017004 (2009).

[19] C. Collignon, S. Badoux, S. A. A. Afshar, B. Michon, F. Laliberté, O. Cyr-Choinière, J.-S. Zhou, S. Licciardello, S. Wiedmann, N. Doiron-Leyraud, and L. Taillefer, Fermi-surface transformation across the pseudogap critical point of the cuprate superconductor La2-xSrxCuO4, Phys. Rev. B **95**, 224517 (2017).

[20] T. Kimura, S. Miyasaka, H. Takagi, K. Tamasaku, H. Eisaki, S. Uchida, K. Kitazawa, M. Hiroi, M. Sera, and N. Kobayashi, In-plane and out-of-plane magnetoresistance in La2-xSrxCuO4 single crystals, Phys. Rev. B **53**, 8733 (1996).

[21] J. Vanacken, L. Weckhuysen, T. Wambecq, P. Wagner, and V. Moshchalkov, High field magnetoresistivity of epitaxial La2-xSrxCuO4 thin films, Physica C **432**, 81 (2005).

[22] T. Yoshida, X. J. Zhou, K. Tanaka, W. L. Yang, Z. Hussain, Z.-X. Shen, A. Fujimori, S. Sahrakorpi, M. Lindroos, R. S. Markiewicz, A. Bansil, S. Komiya, Y. Ando, H. Eisaki, T. Kakeshita, and S. Uchida, Systematic doping evolution of the underlying Fermi surface of La2-xSrxCuO4, Phys. Rev. B **74**, 224510 (2006).

[23] M. Horio, K. Hauser, Y. Sassa, Z. Mingazheva, D. Sutter, K. Kramer, A. Cook, E. Nocerino, O. K. Forslund, O. Tjernberg, M. Kobayashi, A. Chikina, N. B. M. Schröter, J. A. Krieger, T. Schmitt, V. N. Strocov, S. Pyon, T. Takayama, H. Takagi, O. J. Lipscombe *et al.*, Three-Dimensional Fermi Surface of Overdoped La-Based Cuprates, Phys. Rev. Lett. **121**, 077004 (2018).

[24] J. M. Luttinger, Fermi surface and some simple equilibrium properties of a system of interacting dermions, Phys. Rev. **119**, 1153 (1960).

[25] N. P. Ong, Geometric interpretation of the weak-field Hall conductivity in two-dimensional metals with arbitrary Fermi surface, Phys. Rev. B **43**, 193 (1991).

[26] L. B. Ioffe and A. J. Millis, Zone-diagonal-dominated transport in high-Tc cuprates, Phys. Rev. B **58**, 11631 (1998).

[27] R. G. Chambers, The kinetic formulation of conduction problems, Proc. Phys. Soc. A **65**, 458 (1952).

[28] H. Budd, Chamber's Solution of the Boltzmann equation, Phys. Rev. **127**, 4 (1962).

[29] A. A. Abrikosov, *Fundamentals of the Theory of Metals* (North-Holland, Amsterdam, 1988)

[30] K. W. Post, A. Legros, D. G. Rickel, J. Singleton, R. D. McDonald, X. He, I. Božović, X. Xu, X. Shi, N. P. Armitage, and S. A. Crooker, Observation of cyclotron resonance and measurement of the hole mass in optimally doped La2-xSrxCuO4, Phys. Rev. B **103**, 134515 (2021).

[31] A. V. Maharaj, I. Esterlis, Y. Zhang, B. J. Ramshaw, and S. A. Kivelson, Hall number across a van Hove singularity, Phys. Rev. B **96**, 045132 (2017).

[32] N. W. Ashcroft and N. D. Mermin, *Solid State Physics* (Cengage Learning, Mason, OH, 2011).

[33] A. Narduzzo, G. Albert, M. M. J. French, N. Mangkorntong, M. Nohara, H. Takagi, and N. E. Hussey, Violation of the isotropic mean free path approximation for overdoped La2-xSrxCuO4, Phys. Rev. B **77**, 220502(R) (2008).

[34] G. Grissonnanche, Y. Fang, A. Legros, S. Verret, F. Laliberté, C. Collignon, J. Zhou, D. Graf, P. A. Goddard, L. Taillefer *et al.*, Linear-in temperature resistivity from an isotropic Planckian scattering rate, Nature (London) **595**, 667 (2021).

[35] A. Ataei, A. Gourgout, G. Grissonnanche, L. Chen, J. Baglo, M.-E. Boulanger, F. Laliberte, S. Badoux, N. Doiron-Leyraud, V. Oliviero, S. Benhabib, D. Vignolles, J.-S. Zhou, S. Ono, H. Takagi, C. Proust, and L. Taillefer, Electrons with Planckian scattering obey standard orbital motion in a magnetic field, Nat. Phys. **18**, 1420 (2022).

[36] J. Zaanen, Planckian dissipation, minimal viscosity and the transport in cuprate strange metals, SciPost Phys. **6**, 061 (2019).

[37] C. M. Varma and E. Abrahams, Effective Lorentz Force Due to Small-Angle Impurity Scattering: Magnetotransport in High-Tc Superconductors, Phys. Rev. Lett. **86**, 4652 (2001).

[38] E. Abrahams and C. M. Varma, What angle-resolved photoemission experiments tell about the microscopic theory for high-temperature superconductors, Proc. Natl. Acad. Sci. **97**, 5714 (2000).

[39] T. Valla, A. V. Fedorov, P. D. Johnson, Q. Li, G. D. Gu, and N. Koshizuka, Temperature Dependent Scattering Rates at the Fermi Surface of Optimally Doped Bi2Sr2CaCu2O8+δ, Phys. Rev. Lett. **85**, 828 (2000).

[40] A. Kaminski, H. M. Fretwell, M. R. Norman, M. Randeria, S. Rosenkranz, U. Chatterjee, J. C. Campuzano, J. Mesot, T. Sato, T. Takahashi, T. Terashima, M. Takano, K. Kadowaki, Z. Z. Li, and H. Raffy, Momentum anisotropy of the scattering rate in cuprate superconductors, Phys. Rev. B **71**, 014517 (2005).

[41] T. Yoshida, X. J. Zhou, D. H. Lu, S. Komiya, Y. Ando, H. Eisaki, T. Kakeshita, S. Uchida, Z. Hussain, Z.-X. Shen, and A. Fujimori, Low-energy electronic structure of the high-Tc cuprates La2-xSrxCuO4 studied by angle-resolved photoemission spectroscopy, J. Phys.: Condens. Matter **19**, 125209 (2007).

[42] J. Chang, M. Shi, S. Pailhés, M. Månsson, T. Claesson, O. Tjernberg, A. Bendounan, Y. Sassa, L. Patthey, N. Momono, M. Oda, M. Ido, S. Guerrero, C. Mudry, and J. Mesot, Anisotropic quasiparticle scattering rates in slightly underdoped to optimally doped high-temperature La2-xSrxCuO4 superconductors, Phys. Rev. B **78**, 205103 (2008).

[43] J. Chang, M. Maansson, S. Pailhes, T. Claesson, O. Lipscombe, S. M. Hayden, L. Patthey, O. Tjernberg, and J. Mesot, Anisotropic breakdown of Fermi liquid quasiparticle excitations in overdoped La2-xSrxCuO4, Nat. Commun. **4**, 2559 (2013).

[44] M. Abdel-Jawad, M. P. Kennett, L. Balicas, A. Carrington, A. P. MacKenzie, R. H. McKenzie, and N. E. Hussey, Anisotropic scattering and anomalous normal-state transport in a high-temperature superconductor, Nat. Phys. **2**, 821 (2006).

[45] H. U. Özdemir, V. Mishra, N. R. Lee-Hone, X. Kong, T. Berlijn, D. M. Broun, and P. J. Hirschfeld, Effect of realistic out-of-plane dopant potentials on the superfluid density of overdoped cuprates, Phys. Rev. B **106**, 184510 (2022).